Aerodynamic Effects of a Turbulent Flowfield on a Vertically Launched Missile

Richard M. Howard*
Naval Postgraduate School, Monterey, California
M. Peter Rabang†
U.S. Navy, Honolulu, Hawaii
and
Donald P. Roane Jr.‡
U.S. Navy, Bath, Maine

Wind-tunnel tests were performed on a vertically launched surface-to-air missile model to investigate the effects of flowfield turbulence on the side forces induced by nose-generated asymmetric vortices at high angles of attack. The effects of the missile low-aspect-ratio wings on the induced side forces are also investigated. Test angles of attack range from 0 deg to 90 deg at a Reynolds number, based on model diameter, of 1.1×10^5, and at a Mach number of 0.1. Three body configurations and five flowfield conditions are tested. Increased freestream turbulence at the boundary-layer scale greatly reduces the side forces, and the initial tendency of an increase in intensity at a vortex scale is to stabilize the asymmetric behavior and to maintain the side force magnitude. Increased levels of turbulence reduces the side forces, but magnitudes remain significant. For ambient turbulence conditions, side forces are maintained at approximately the same levels with and without wings.

Nomenclature

C_N = normal force coefficient, $N/[(\rho U_\infty{}^2/2)S]$
C_Y = side force coefficient, $Y/[(\rho U_\infty{}^2/2)S]$
D = model body diameter
L_e = turbulence dissipation length scale
M = grid mesh width
N = normal force
Re = Reynolds number, $\rho U_\infty D/\mu$
S = reference area, $\pi D^2/4$
Tu = turbulence intensity, u'/U_∞
U = streamwise mean velocity
U_∞ = freestream velocity
u' = root-mean-square of streamwise fluctuating velocity component
v' = root-mean-square of transverse fluctuating velocity component
x = streamwise coordinate
Y = side force
α = angle of attack
ϕ = roll angle
μ = coefficient of molecular viscosity
ρ = air density

Introduction

Vertically Launched Missile

THE recent introduction of a vertical launch capability for ships carrying surface-to-air missiles represents a major advancement in weapon system reliability and flexibility.[1] A characteristic of vertically launched missiles is their inability to point at the target intercept point prior to launch. As a result, the missile must be maneuvered to its intercept trajectory. But, the initial launch speed of the missile is relatively low, and the aerodynamic surfaces are not yet sufficient for maneuvering. During this time, the missile is subject to potentially significant crosswinds, resulting in an effective high angle of attack. The requirements for certain trajectories also place high angle-of-attack demands on the vertically launched missile. Angles of attack may reach up to 50 deg during turnover maneuvers.[2]

The existence of an induced side force on slender bodies due to the formation of asymmetric vortices at high angles of attack has been characterized by numerous investigators; only a few of the most recent are given for reference.[3-5] A review of past work is given by Paul.[6] Unpredictable side forces may be generated under certain flow conditions for the vertically launched missile, which pose a potential threat to flight stability. Additionally, the flowfield may contain some degree of turbulence. The surface layer of the marine atmospheric boundary layer (approximately the first 50–100 m) may have a turbulence intensity of 10–15% of the mean wind speed,[7,8] and other large-scale turbulence due to flow over the ship superstructure—commonly called ship airwake turbulence—may be present. The expected length scales of the atmospheric turbulence would be on the order of 100 m; yet the energy cascade of turbulence requires turbulent eddies to exist in size over orders of magnitude. The degree to which small-scale turbulence is present in the marine atmosphere of a scale that may affect the development of vortices from the missile nose is largely unknown.[8] The current study considers the effects on generated side forces of elevated turbulence levels and increased turbulence scales generated in a wind-tunnel environment.

Asymmetric Vortex Formation

The general consensus of previous work concerning the formation of asymmetric vortices at high angles of attack is that the phenomenon is extremely Reynolds-number dependent; it has been noted that the generation of strong side forces (normalized by the normal force) occurs in the critical Reynolds

Received Oct. 31, 1988; presented as Paper 89-0329 at the AIAA 27th Aerospace Sciences Meeting, Reno, NV, Jan. 9–12, 1989; revision received April 3, 1989.

*Assistant Professor, Department of Aeronautics and Astronautics. Member AIAA.
†Lieutenant, U.S. Navy; Operations Officer, USS *Harold E. Holt*.
‡Lieutenant, U.S. Navy; Weapons Control Officer, USS *Normandy*.

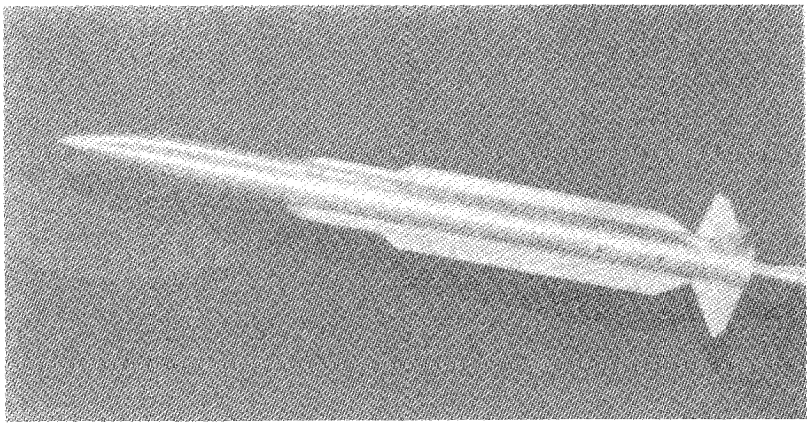

Fig. 1 Vertically launched surface-to-air missile model.

number regime, where the body experiences subcritical (laminar) vortex separation on one side and critical separation on the other.[3] This regime is usually considered to range between Reynolds numbers of about 10^5 and 10^6, based on a two-dimensional flow analogy to crossflow over circular cylinders. But other recent work[4] supports the proposition that the principal cause of vortex asymmetry is a hydrodynamic instability of the inviscid flowfield. The vortices, increasing in strength with angle of attack and crowding together for a sufficiently large value of nose fineness ratio, apparently interact with the surrounding potential flowfield to stabilize in a steady or quasi-steady asymmetric configuration. This hypothesis is supported by flow visualization indicating that at low Reynolds numbers (3.0×10^5), large asymmetries in the surface-flow patterns exist when laminar separation occurs over the length of slender forebodies.[4] Tests conducted with ogive length-to-diameter ratios of 2.0 and 3.5 suggest the stronger mechanism for producing side forces occurs at Reynolds numbers greater than and less than those in the critical regime, with the second mechanism in the transitional separation regime being fairly weak.[9,10] The complexity of the phenomenon is apparent in the difficulty with which recent attempts at advances can be made in resolving a dominant mechanism.[11] Similarities in vortex asymmetries over highly swept delta wings to those over ogive forebodies suggest that asymmetry in the separation characteristics of a body of revolution may not necessarily be an essential feature of vortex asymmetry.[12]

A vortex-switching phenomenon has also been observed[13,14] in which, under certain flow conditions, the vortex pattern was found to rapidly switch from an almost symmetric configuration to a highly asymmetric one. This phenomenon may either relate to a fluctuation in the separation nature and location on the sides of the slender body, or to the possibility of a second inviscid solution in the leeward flowfield. In either case there is no doubt that the contribution of boundary-layer asymmetries to the asymmetric vortex formation is significant at critical Reynolds numbers, though perhaps not principal.

Effects of Wings and Freestream Turbulence

Though many studies have been performed considering slender bodies at high angles of attack, little work has been done treating the influence of realistic wing planforms on the formation of asymmetric vortices. The surface-to-air missile modeled (described below) possesses long, very-low-aspect-ratio cruciform wing-and-strake lifting surfaces, running over half the body length (Fig. 1). A model with a similar wing and tail configuration was tested[2] at a Mach number of 0.5 up to angles of attack of 50 deg for roll angles of 0 deg and 45 deg. A comparison to the body-only case showed a decrease in the induced side force from a maximum C_Y value of about 3 to a value of about 0.8 at $\phi = 0$ deg, and a decrease to a maximum value of about 0.5 for $\phi = 45$ deg. The authors note that "the out-of-plane forces were largely eliminated by the presence of the strakes [wings]."[2] The mechanism by which the presence of the wings actually influences the nose-generated asymmetric vortices is not discussed.

Likewise, little work has been done considering the effect of increased levels of flowfield turbulence on the vortex formation. Ericsson and Reding[15] note that the critical Reynolds number at which the induced side force is maximized will vary from wind tunnel to wind tunnel due to the effect of freestream disturbances and tunnel noise on boundary-layer transition. For studies of boundary-layer response, reference is made to previous studies of more typical two-dimensional boundary-layer behavior, rather than to any studies on slender bodies at high angles of attack. Lamont and Hunt[16] ascribe a flow-switching unsteadiness, observed in time-dependent pressure measurements 7 diameters from the nose, to freestream turbulence. The cylinder has an ogive length-to-diameter ratio of 2, and the flow conditions were a Reynolds number of $1.1.\times 10^5$ (based on slant distance) and $\alpha = 30$ deg. Dexter and Hunt[17] demonstrated that freestream turbulence can have a large effect on the transient surface pressures of the ogive cylinder in work performed in a wind tunnel with an ambient turbulence level of 0.01%. Wardlaw and Yanta[18] experimented with a turbulence-generating screen that increased the freestream turbulence to a level of about 2%. It was noted that the surface pressures measured with and without the screen installed were similar, with slightly higher standard deviation values with the screen. The side force distribution of peak values with roll angle did not alter qualitatively, though the maximum peak values of C_Y increased by about 10%.

Definition of Study

It was decided to perform a study of the effects of a realistically configured wing planform and of freestream turbulence on the generation of asymmetric vortices and the resulting side force. A desired outcome of current and future research in this area is a better understanding of the causal mechanism of the phenomenon—whether it is a stronger function of the boundary-layer transitional behavior or of the vortex interaction in the inviscid flowfield.

Current Experimental Program

A wind-tunnel study of normal forces and induced side forces over a range of angles of attack of up to 90 deg has been performed for a generic, vertically launched, surface-to-air missile (VLSAM). Runs were made with four turbulence-generating grids to observe the effects of freestream turbulence intensities and scales on the formation of asymmetric vortices. Body configurations compared were body-only, body-wings-tail at 0-deg roll angle (wings-tail in a "+" orien-

tation), and body-wings-tail at 45-deg roll angle (wings-tail in an "×" orientation). Flow visualization studies were initiated using smoke and a laser light sheet to illuminate the steady asymmetric behavior.

Model

The VLSAM is representative of current ship-based, vertically launched, surface-to-air missiles. The model is of a cruciform tail-control missile with narrow strakes and long strake-like dorsal wings.[19] The size and shape of such a missile is unclassified information.[20] The model diameter is 1.75 in., the length is 22.85 in., and the ogive length-to-diameter ratio is 2.29; the model represents approximately a one-seventh-scale missile. Forces and moments were measured by an internal sting-mounted, six-component, strain-gage balance. For minimum tunnel interference, the support system was constructed to pivot the model at its approximate center for angle-of-attack changes.

Test Conditions

The wind tunnel used for the experiments at the Naval Postgraduate School has a test section measuring 28 by 45 in., with a contraction ratio of approximately 10. Because of the extreme blockage of the turbulence grids (20% for three of the four grids), pressure losses in the tunnel limited the available Reynolds number, based on model diameter, to about 1.1×10^5. This particular Reynolds number lies at the lower end of the critical Reynolds number range, where a change from laminar to turbulent separation might be expected to occur over the missile model.[15] Keener[4] notes for his tests that at a Reynolds number of 3×10^5, only subcritical, laminar-type separation occurred on both sides of the forebody (though not necessarily symmetrically), while vortex asymmetry existed in the leeward flowfield. In the current experiment, one might expect the separation characteristics (at least for ambient turbulence) to be similar for both sides of the missile body. The existence of a strong induced side force in this case would tend to support the hypothesis that a critical/subcritical separation behavior might not be a requirement for asymmetric vortical flow.

Data were corrected for solid blockage,[21] but no correction was made for sting interference effects. Tail control surfaces were fixed. Side and normal force coefficients were referred to an area based on the body diameter. The six-component balance was calibrated at the NASA Ames Research Center prior to use at the Naval Postgraduate School; check calibrations were performed with the balance in place in the wind tunnel.

Turbulence Grids

Each grid was located 73 in. upstream of the pitch axis of the model support system. Three square-mesh, square-bar, biplanar grids and a single square-mesh, round-wire grid were used. See Table 1 for grid geometry. The grids were located at the downstream end of the contraction section of the wind-tunnel settling chamber. Grids of this design have been found to successfully generate nearly isotropic turbulence.[22] With this grid design, the longitudinal turbulence intensity is about 5% greater than the lateral and transverse components.[23]

Turbulence Intensities and Scales

Hot-wire anemometry was used for longitudinally mapping the turbulence generated in the wind tunnel. A single-sensor probe was positioned in the center of the tunnel and traversed along the centerline from the grids through the test section. A turbulence intensity of 0.23% was found for the test section with no grids installed at the test Reynolds number. This value is typical of common closed-circuit wind tunnels.

Table 1 Grid Specifications[a]

Grid	M	d, bar diam.	M/d	Material
1	5.00	1.00	5	wood
2	3.75	0.75	5	wood
3	2.50	0.50	5	wood
4	1.00	0.0625	16	wire

[a]Dimensions in inches.

As noted for grid-generated turbulence, the ratio of u' to v' is approximately 1.05. This relation was used to extract the turbulence intensity based on the fluctuation in the freestream direction using a single hot-wire sensor. Figure 2 shows the measured intensities for the four grids plotted against distance from the grids. The crossover between grids 1 and 2 near the grid location is due to the lateral position of the sensor with respect to the grid bars. Previous work has shown that a minimum distance of 6 mesh widths is required for the turbulent flow to achieve reasonable homogeneity[23]; the distance from the grid location to the missile nose for the largest mesh grid is 12 mesh widths. The turbulence intensities at the missile nose for the four grids were 3.80% for grid 1, 3.12% for grid 2, 2.14% for grid 3, and 0.53% for grid 4.

Meier[24] describes a method for correlating the decay of the turbulence intensity with the distance downstream of a turbulence-generating grid. Hancock and Bradshaw[22] and Castro[23] link the turbulence dissipation length scale L_e with the decay of turbulence intensity. Therefore, length scales representative of the turbulent dissipation eddies can be estimated from the turbulence intensity measurements.

For grid-generated turbulence, the intensity decreases as

$$[(u'/U)^2]^{-0.8} = A\,(x/M - B) \tag{1}$$

where A and B are constants to be determined for each grid.[23] The turbulent dissipation length scale is related to the intensity by[23]

$$U\,\frac{\mathrm{d}(u'^2)}{\mathrm{d}x} = -(u')^{3/2}/L_e \tag{2}$$

giving length scales varying with downstream distance as

$$L_e/M = 0.8[A^{-0.625}][x/M\text{-}B]^{0.375} \tag{3}$$

Figure 3 indicates the dissipation length scales for the four grids. Note that the representative size increases gradually with downstream distance, due to the rapid dissipation of the smaller scales with viscosity. The length scales at the missile nose are 1.7 in. for grid 1, 1.5 in. for grid 2, 1.0 in. for grid 3, and 0.25 in. for grid 4. Table 2 summarizes the grid-related turbulence parameters at the missile nose. The scale for the largest mesh grid, grid 1, is identical to the body diameter; for vortical flow about a missile at high angles of attack, one might expect a turbulence scale on the order of the body diameter to most greatly influence the separation phenomenon. The smallest grid, grid 4, produces a scale of about 15% of the body diameter.

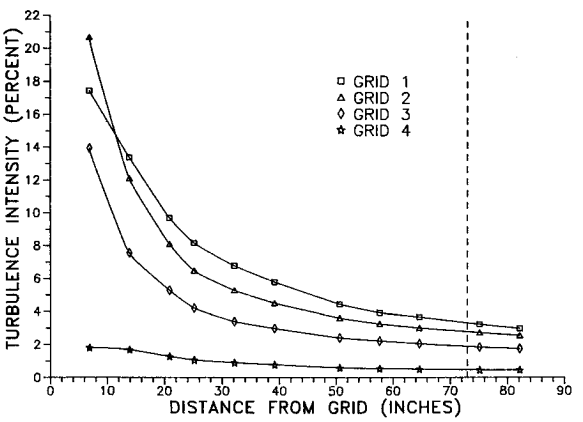

Fig. 2 Turbulence intensities measured for grids.

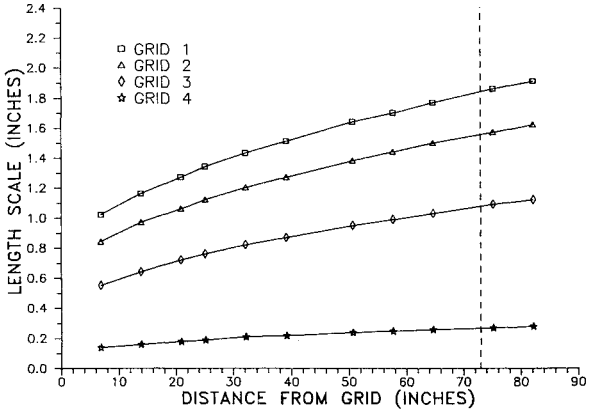

Fig. 3 Turbulence length scales determined for grids.

Table 2 Grid turbulence parameters at the missile nose

Grid	Intensity, %	L_e, in.	L_e/D
1	3.80	1.7	1.0
2	3.12	1.5	0.85
3	2.14	1.0	0.5
4	0.53	0.25	0.15
no grid	0.23	—	—

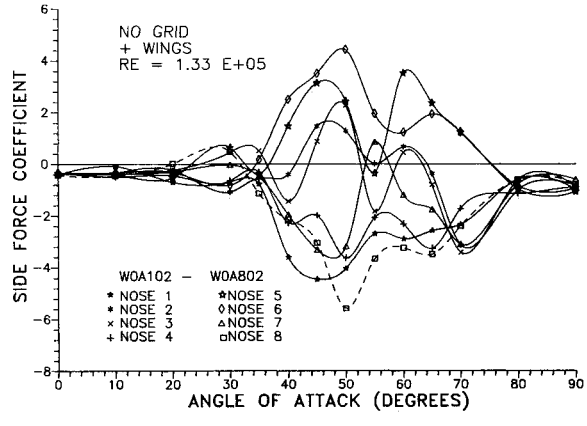

Fig. 4 Side force with nose roll angle.

Results

Nose Position

The behavior of the nose-generated vortical flow has been found by numerous investigators to be extremely sensitive to the nose roll angle. Apparently, microasymmetries in the ogive nose geometry are sufficient to influence the direction of the resulting side force, as well as its magnitude, over the range of angles of attack. Figure 4 shows the resulting side force coefficients for roll angles varied at 45-deg increments. For these cases, the body-wings-tail is fixed at 0-deg roll angle, while the nose is rotated through the roll angle variation. Such a procedure eliminated any effect from body roll angle.

For all of the nose roll angles, nonzero side forces are seen to begin at about 20-deg angle of attack, and to remain until about 80 deg. Nose 1 indicates 0-deg roll angle referenced to an arbitrary starting point with each succeeding number indicating an increase in roll angle of 45 deg. A maximum positive C_Y of about 5.0 is reached at a roll position of 225 deg (nose 6) and a maximum negative C_Y of about -6.0 is reached at a roll angle of 315 deg (nose 8); nose 8 was then used for the remainder of the tests to produce the maximum possible side force during the experiments.

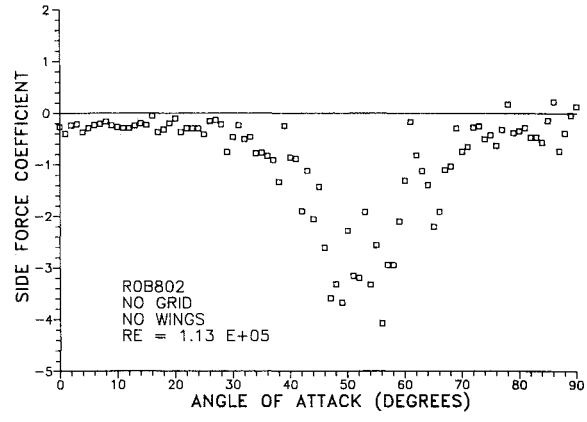

Fig. 5 Side force vs angle of attack, no grid, body only.

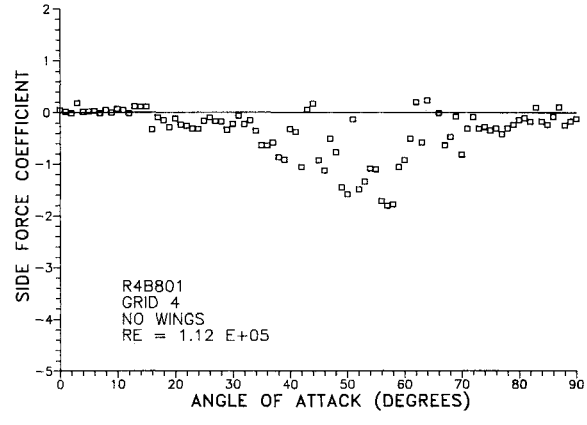

Fig. 6 Side force vs angle of attack, grid 4, body only.

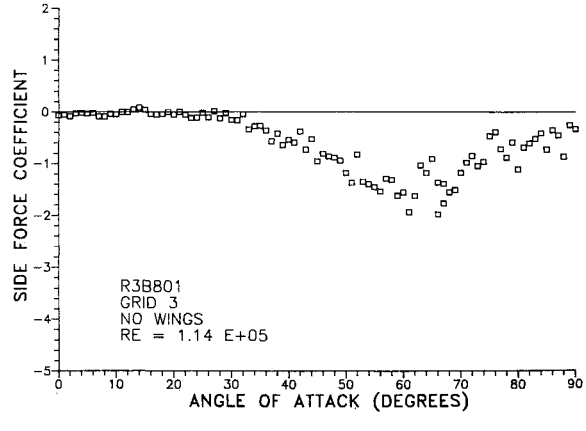

Fig. 7 Side force vs angle of attack, grid 3, body only.

Series of runs were made for the body-only case and for the body-wings-tail configuration at 0-deg and 45-deg roll angle. Each configuration was tested over the range of incidence angles from 0 deg to 90 deg for the four grids and for the ambient no-grid case.

Body Only

Figure 5 shows the results of the missile body with no turbulence grid; the turbulence intensity is about 0.23%, the nominal wind-tunnel value. As representative dissipation length scales were determined from the decay of grid-generated turbulence, no length scale was estimated for this intensity level.

Nonzero induced side forces come into play at about 25 deg angle of attack, and a maximum C_Y of about -4.2 is reached around 50 deg. A comparison of the side force coefficients

with those for the case with the smallest level of elevated turbulence, shown in Fig. 6 for grid 4, indicates a reduction due to the increased turbulence level to a maximum value of about -2.0 at the same angle of attack. At the smaller length scales, an increased freestream turbulence has the consequence of effectively increasing the Reynolds number. Figure 7 shows the side force with grid 3; note that the maximum side force coefficient has remained the same and the main difference between the two cases is that the data have shifted to slightly higher angles of attack. The angle of onset of asymmetric vortices is about 30 deg. Between these two cases, the turbulence intensity and length scale have both increased by a factor of 4. The latter data also tend to show less scatter, indicating that increased turbulence at larger scales acts to reduce the unsteadiness of the asymmetric vortex flow.

Figure 8 shows a reduction in the side forces to a maximum value of about -1.3 for the increase in turbulence parameters of 50%. The scatter in data due to the vortex unsteadiness remains fairly high. Figure 9 at the maximum turbulence intensity of 3.80% and length scale of 1.7 in. shows similar results, with side force coefficient values remaining smaller than -1.0. For the body-only case, an increase in intensity and scale tends to reduce the induced side forces and to shift the range of action to slightly higher incidence angles. An initial speculation is that since the dissipation vortices of turbulence in the last case are of the model diameter size, the mechanism tending to reduce the vortex asymmetry is an interaction between the forebody/body-generated vortices and those of the freestream turbulence, rather than a premature transitioning of a subcritical boundary layer.

Body-Wings-Tail at 0-Deg Roll Angle

Figure 10 shows the results on side force of adding the lifting and control surfaces to the missile body. Side forces begin to be generated at about 20 deg and continue until about 80 deg. A maximum value of about -4.6 is reached at an angle of attack of 46 deg. Evident is the extreme scatter of data in the region of strong induced side forces.

A comparison of Figs. 10 and 5 indicates a result of the low-aspect-ratio wings is to widen the range of large values of C_Y. Overall the behavior is similar, with a slightly larger scatter in the data for the winged case. For the winged case, a reversal in side force at the angle of initial onset has taken place. Contrary to the results noted by other investigators,[2] the induced side force appears to be maintained and strengthened by the addition of long cruciform fin-like wings in the 0-deg roll angle orientation. Currently, it is unknown whether the vortices being shed from the wings and strakes act to energize the asymmetric forebody/body vortices, or whether the wings and strakes themselves generate a vortex asymmetry.[13] Future tests will investigate the flowfield interactions directly with local measurements.

As can be seen in Fig. 11, the addition of grid 4 reduces the magnitude of the side forces to levels almost identical to the no-grid case for body only (Fig. 5). A small reversal in the side force direction can be noted at the initial onset of nonzero side force. A distinctive change in behavior appears with the addition of grid 3, seen in Fig. 12. Recall that grid 4 doubles the turbulence intensity from its nominal no-grid value; grid 3 quadruples the level of intensity (from 0.53 to 2.14%) as well as the dissipation length scale (from 0.25 to 1.0 in.). Whereas the case with grid 4 showed a behavior similar to the no-grid case but at a slightly reduced magnitude, the case with grid 3 shows a change in side force response, noted by the following:

1) There is no reversal of force direction at the initial onset of nonzero side force.

2) The maximum side force has increased back to a level identical with the no-grid case.

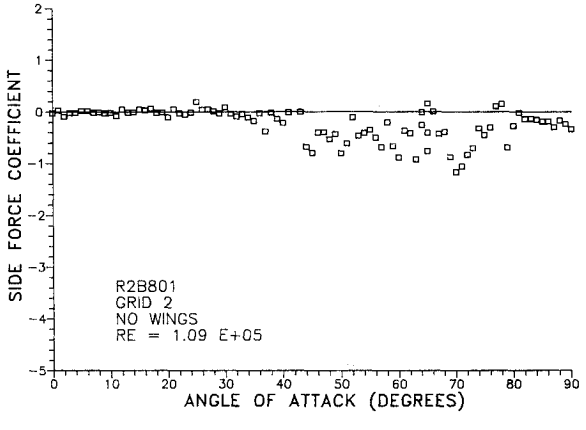

Fig. 8 Side force vs angle of attack, grid 2, body only.

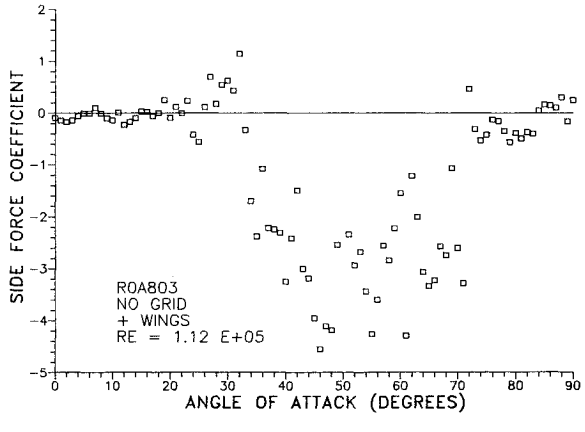

Fig. 10 Side force vs angle of attack, no grid, "+" configuration.

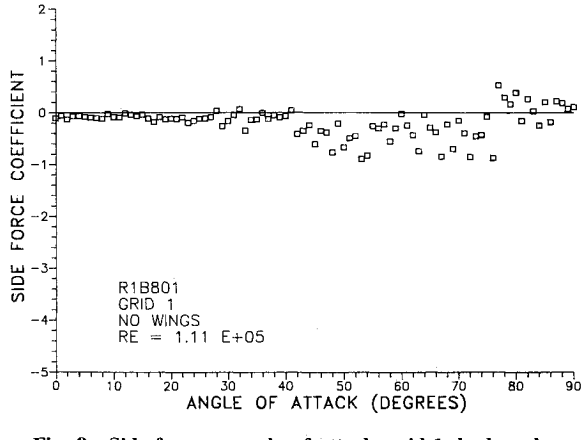

Fig. 9 Side force vs angle of attack, grid 1, body only.

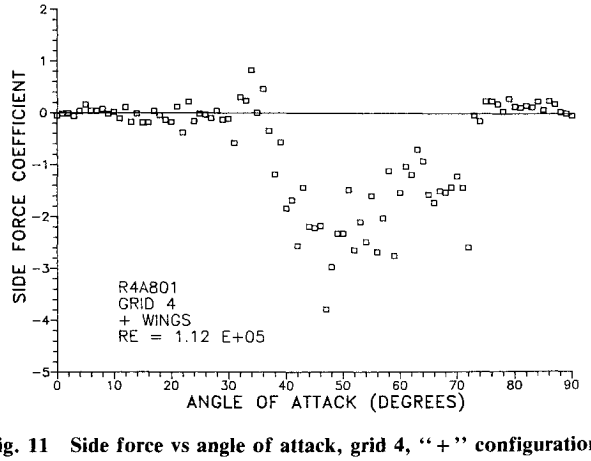

Fig. 11 Side force vs angle of attack, grid 4, "+" configuration.

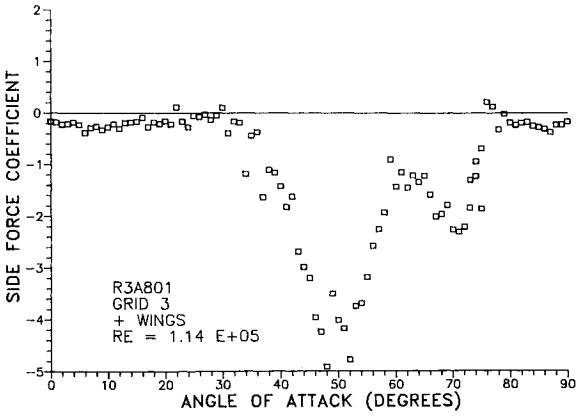

Fig. 12 Side force vs angle of attack, grid 3, "+" configuration.

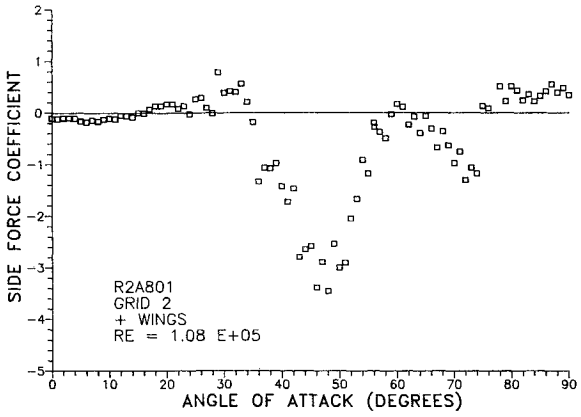

Fig. 13 Side force vs angle of attack, grid 2, "+" configuration.

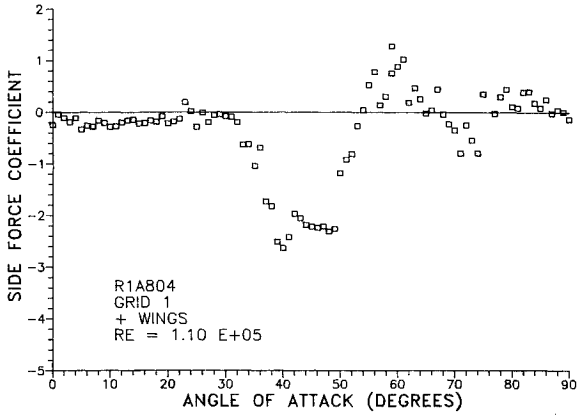

Fig. 14 Side force vs angle of attack, grid 1, "+" configuration.

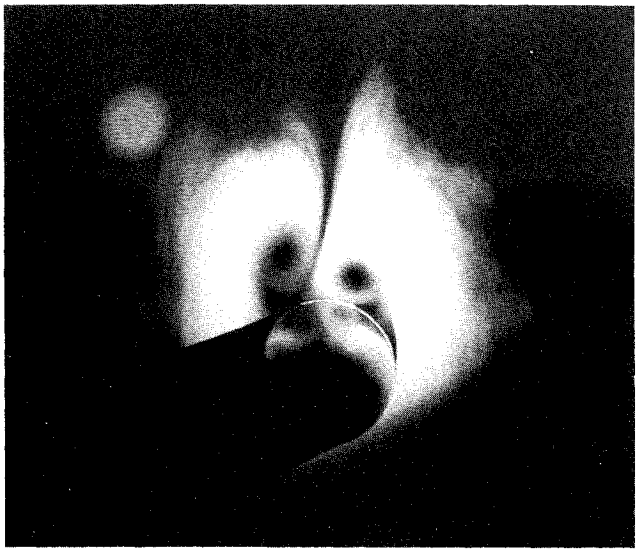

Fig. 15 Flow visualization of asymmetric vortices, $\alpha = 60$ deg.

3) There is much less scatter in the data, indicating the vortex wake structure is steadier than for the no-grid or the grid 4 case.

A comparison of Figs. 6 and 7 for the body-only configuration indicates that the grid 3 case in that instance produced smoother data, with a slightly higher maximum value of C_Y. Two general conclusions that might be drawn from the two-body configurations, with and without wings, are as follows.

1) An increase in turbulence intensity with a length scale on the order of the boundary-layer scale tends to reduce the magnitude of the induced side force, while keeping the same shape of the response with incidence angle as for the ambient case.

2) An increase in turbulence intensity with a length scale on the order of the nose-generated-vortex scale tends to delay the onset of induced side force, to steady the asymmetric vortex formation and to leave the maximum value of C_Y more or less unaltered.

Further increasing the intensity and length scale tends to reduce the maximum value of C_Y (-3.6 for grid 2, Fig. 13, to -2.6 for grid 1, Fig. 14), while maintaining the general shape of the response first seen when vortex-scale turbulence was introduced.

A comparison of the runs for the cases of the body-only and the body-wings-tail configurations shows that the addition of wings and strakes typical of a vertically launched missile tends to preserve the induced side force over all levels of turbulence intensities and length scales treated. For the largest-mesh grid, for example, the maximum value of C_Y is about 2.5 times as high for the winged case as for the body-only case. Evidently the wing-and-strake vortices, either by direct interaction or by their own asymmetry, can maintain a strong induced side force at a Reynolds number of 1.1×10^5, even at elevated turbulence levels.

Body-Wings-Tail at 45-Deg Roll Angle

An identical set of runs was made for the missile at a roll angle of 45 deg, placing the wings and tail in an "×" orientation. The trends are similar to those shown previously, with regards to the effects of freestream turbulence. Space limitations prevent a presentation of the results. For the complete results, see Ref. 25.

Flow Visualization

A smoke probe and laser light sheet were used to illustrate the nature of the vortical behavior. Figure 15 shows the steady asymmetric vortices at an angle of attack of 60 deg at a location 3 diameters from the nose. Sketches of similar behavior can be found in Keener.[4]

Conclusions and Recommendations

Wind-tunnel tests were performed on a vertically launched surface-to-air missile model over a range of angles of attack from 0 deg to 90 deg at a Reynolds number based on diameter of 1.1×10^5. Three configurations were tested: body-only, body-wings-tail at 0-deg roll angle, and body-wings-tail at 45-deg roll angle. Five flowfield conditions were treated: the nominal ambient wind-tunnel conditions, and four conditions with grid-generated turbulence giving a range of turbulence in-

tensities and dissipation length scales. The following conclusions were reached:

1) Strong induced side forces exist at a Reynolds number that, according to previous work,[4] could be expected to have laminar separation on both sides of the slender body. This result supports the hypothesis that critical/subcritical separation conditions are not a requirement for the formation of asymmetric vortices. It should be made clear, though, that no direct investigation into the body separation behavior by surface pressures or flow visualization was conducted.

2) Side forces were maintained at approximately the same magnitudes for the body-only and the body-wings-tail configurations at ambient wind-tunnel turbulence levels. Data generally are scattered, indicative of unsteady vortical flow, though with a determinable mean.

3) In no case was a mirror-image flow switching found for the chosen nose orientation. Within a band of scatter, the data were repeatable.

4) For the body-only case, an increase in turbulence intensity tends to greatly reduce the maximum induced side force. Yet the increase in turbulence intensity from 0.23 to 0.53% had a much greater effect than the increase from 0.53 to 2.14%, the latter with an accompanying scale increase from 0.25 to 1.0 in. It is believed that the initial reduction (with a high level of unsteadiness) is due to changes in the transitional boundary-layer behavior, while further increases at larger scales have little influence on the boundary-layer behavior.

5) The initial effect of increased turbulence on the winged configurations is to reduce the magnitude of the side force while maintaining the same level of vortex flow unsteadiness. As the turbulence is further increased to very large intensities and to larger length scales, side forces increased or maintained at the same level and the force data became smoother, indictating a steadier vortical flow.

These results indicate that the effect of the initial turbulence intensity increase (at roughly a boundary-layer scale) is to modify the boundary-layer separation characteristics at the sides of the missile model body. Further increases in intensity and length scales (on the order of the nose-generated vortices) appear to directly impact the vortex flowfield.

Acknowledgments

This research was supported by the Standard Missile Program Office of the Naval Surface Warfare Center and the Department of Aeronautics and Astronautics at the Naval Postgraduate School. The authors thank the NASA Ames Research Center for the loan and calibration of the six-component balance that was arranged through the Navy-NASA Joint Institute of Aeronautics. Thanks go to Jack Brownson, Jim McMahon, Chuck Prunty, and Doug McMurchy at NASA Ames for their assistance. Special thanks go to John Moulton for construction of the missile model, and to Joe Chlebanowski for development of the flow visualization equipment. The authors lastly thank the reviewers for their helpful suggestions and insights.

References

[1]Friedman, N., "Naval Vertical Launch Missile Systems," *Military Technology,* Vol. 9, May 1985, pp. 24-31.

[2]Gregoriou, G. and Knoche, H. G., "High Incidence Aerodynamics of Missiles during Launch Phase," Messerschmitt-Bolkow-Blohm Rept. UA-523/80, Jan. 1980.

[3]Reding, J. P. and Ericsson, L. E., "Re-examination of the Maximum Normalized Vortex-Induced Side Force," *Journal of Spacecraft and Rockets,* Vol. 21, Sept.-Oct. 1984, pp. 433-440.

[4]Keener, E. R., "Flow-Separation Patterns on Symmetric Forebodies," NASA TM-86016, Jan. 1986.

[5]Yongnian, Y., Xinzhi, Y., and Jianying, L., "Active Control of Asymmetric Forces at High Incidence," *Journal of Aircraft,* Vol. 25, Feb. 1988, pp. 190-192.

[6]Paul, B. P., Jr., "An Investigation of the Flow About an Ogive Cylinder at High Angles of Incidence," von Karman Institute for Fluid Dynamics, Rhode-Saint-Genese, Belgium, Proj. Rept. 1981-21, June 1981.

[7]Healey, J. V., "Simulating the Helicopter-Ship Interface as an Alternative to Current Methods of Determining the Safe Operating Envelopes," Naval Postgraduate School, Monterey, CA, NPS67-86-003, Sept. 1986.

[8]Tieleman, H. W., "A Survey of the Turbulence in the Marine Surface Layer for the Operation of Low Reynolds Number Aircraft," Virginia Polytechnic Inst. and State Univ., Blacksburg, VA, VPI-E-85-10, March 1985.

[9]Lamont, P. J., "Pressures Around an Inclined Ogive Cylinder with Laminar, Transitional, or Turbulent Separation," *AIAA Journal,* Vol. 20, Nov. 1982, pp. 1492-1499.

[10]Lamont, P. J., "The Complex Asymmetric Flow Over a 3.5D Ogive Nose and Cylindrical Afterbody at High Angles of Attack," AIAA Paper 82-0053, Jan. 1982.

[11]Champigny, P., "Reynolds Number Effect on the Aerodynamic Characteristics of an Ogive-Cylinder at High Angles of Attack," AIAA Paper 84-2176, Aug. 1984.

[12]Keener, E. R. and Chapman, G. T., "Similarity in Vortex Asymmetries over Slender Bodies and Wings," *AIAA Journal,* Vol. 15, Sept. 1977, pp. 1370-1372.

[13]Clark, W. C. and Nelson, R. C., "Body Vortex Formation on Missiles at High Angles of Attack," AIAA Paper 76-65, Jan. 1976.

[14]Deffenbaugh, F. D. and Koerner, W. G., "Asymmetric Vortex Wake Development on Missiles at High Angles of Attack," *Journal of Spacecraft and Rockets,* Vol. 14, March 1977, pp. 155-162.

[15]Ericsson, L. E. and Reding, J. P., "Steady and Unsteady Vortex-Induced Asymmetric Loads on Slender Vehicles," *Journal of Spacecraft and Rockets,* Vol. 18, March-April 1981, pp. 97-109.

[16]Lamont, P. J. and Hunt, B. L., "Pressure and Force Distributions on a Sharp-Nosed Circular Cylinder at Large Angles of Inclination to a Uniform Subsonic Stream," *Journal of Fluid Mechanics,* Vol. 76, Pt. 3, Aug. 1976, pp. 519-559.

[17]Dexter, P. C. and Hunt, B. L., "The Effects of Roll Angle on the Flow over a Slender Body of Revolution at High Angles of Attack," AIAA Paper 81-0358, Jan. 1981.

[18]Wardlaw, A. B. and Yanta, W. J., "Multistable Vortex Patterns on Slender, Circular Bodies at High Incidence," *AIAA Journal,* Vol. 20, April 1982, pp. 509-515.

[19]Lindsey, G. H. and Redmon, D. R., *Tactical Missile Design,* AE 4704 Class Notes, Naval Postgraduate School, Monterey, CA, 1980.

[20]OPNAVINST S5513.3B, Enclosure (63), ID 03B-63.

[21]Pope, A and Harper, J. J., *Low-Speed Wind Tunnel Testing,* Wiley, New York, 1966, pp. 105-107.

[22]Hancock, P. E. and Bradshaw, P., "The Effect of Free-Stream Turbulence on Turbulent Boundary Layers," *Journal of Fluids Engineering,* Vol. 105, Sept. 1983, pp. 284-289.

[23]Castro, I. P., "Effects of Free Stream Turbulence on Low Reynolds Number Boundary Layers," *ASME Transactions,* Vol. 106, Sept. 1984, pp. 298-306.

[24]Meier, H. U., "The Response of Turbulent Boundary Layers to Small Turbulence Levels in the External Free Stream," International Council of the Aeronautical Sciences Paper 76-05, Oct. 1976.

[25]Howard, R. M., Rabang, M. P., and Roane, D. P., Jr., "Aerodynamic Effects of a Turbulent Flowfield on a Vertically Launched Missile," AIAA Paper 89-0329, Jan. 1989.